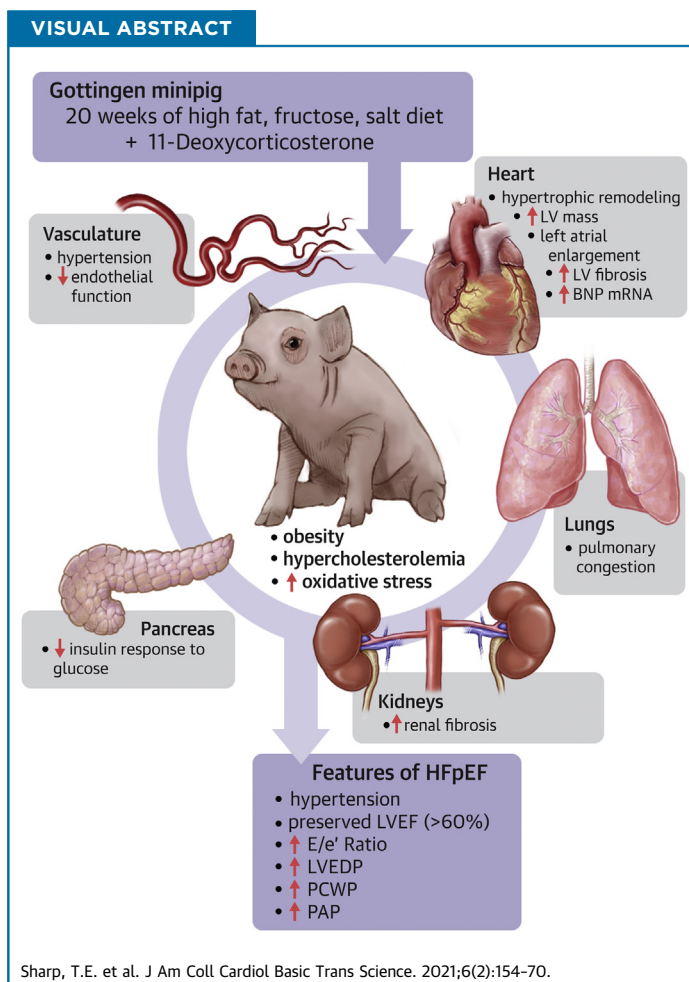


NOVEL TRANSLATIONAL MODELS

Novel Göttingen Miniswine Model of Heart Failure With Preserved Ejection Fraction Integrating Multiple Comorbidities



Thomas E. Sharp III, PhD,^a Amy L. Scarborough, BS,^a Zhen Li, PhD,^a David J. Polhemus, PhD,^a
Hunter A. Hidalgo, BS,^{a,b} Jeffery D. Schumacher, DVM,^c Timothy R. Matsuura, PhD,^d J. Stephen Jenkins, MD,^e
Daniel P. Kelly, MD,^d Traci T. Goodchild, PhD,^{a,b} David J. Lefer, PhD^{a,b}



HIGHLIGHTS

- A large animal model that recapitulates the clinical heterogeneity of HFpEF has been developed.
- Multiple comorbidities, including obesity, hypercholesterolemia, pre-diabetic phenotype, as well as pulmonary and systemic arterial hypertension, were induced in adult female Göttingen minipigs by mineralocorticoid excess and a diet high in cholesterol, fat, fructose, and salt.
- Severity of each comorbidity was titrated, such that marked left ventricular and left atrial diastolic dysfunction, profound left ventricular concentric remodeling, impaired coronary vasorelaxation, and extensive multiorgan fibrosis were achieved over a relatively short time.
- This novel heart failure model was generated in Göttingen minipigs to allow for translational studies of novel pharmacological agents and for human-sized device testing in adult-aged animals.
- This novel "multihit" minipig heart failure model enabled investigations into the pathology of HFpEF without the confounding effects inherent with invasive surgical procedures or the administration of agents that induce hypertension and end-organ damage in an artificial manner.

SUMMARY

A lack of preclinical large animal models of heart failure with preserved ejection fraction (HFpEF) that recapitulate this comorbid-laden syndrome has led to the inability to tease out mechanistic insights and to test novel therapeutic strategies. This study developed a large animal model that integrated multiple comorbid determinants of HFpEF in a miniswine breed that exhibited sensitivity to obesity, metabolic syndrome, and vascular disease with overt clinical signs of heart failure. The combination of a Western diet and 11-deoxycorticosterone acetate salt–induced hypertension in the Göttingen miniswine led to the development of a novel large animal model of HFpEF that exhibited multiorgan involvement and a full spectrum of comorbidities associated with human HFpEF. (*J Am Coll Cardiol Basic Trans Science* 2021;6:154-70) © 2021 The Authors. Published by Elsevier on behalf of the American College of Cardiology Foundation. This is an open access article under the CC BY-NC-ND license (<http://creativecommons.org/licenses/by-nc-nd/4.0/>).

ABBREVIATIONS AND ACRONYMS

DBP	= diastolic blood pressure
DOCA	= 11-deoxycorticosterone acetate
EC₅₀	= half-maximal effective concentration
EF	= ejection fraction
HDL	= high-density lipoprotein
HFpEF	= heart failure with preserved ejection fraction
HFrEF	= heart failure with reduced ejection fraction
LDL	= low-density lipoprotein
IVGTT	= intravenous glucose tolerance test
LV	= left ventricle
PCWP	= pulmonary capillary wedge pressure
SBP	= systolic blood pressure
TC	= total cholesterol
WD	= Western diet

Heart failure with preserved ejection fraction (HFpEF) has emerged as cardiovascular medicine's most complex, comorbidity-laden, heterogeneous disease. The increasing prevalence of HFpEF in an obese, diabetic, hypertensive, aging population, coupled with lack of effective treatments, further complicates this critical public health problem (1). Although complex in its multiorgan pathophysiology, all patients who experience HFpEF exhibit increased left ventricular (LV) filling pressure and reduced exercise tolerance with a preserved LVEF (2,3). Despite the clear cardiac indexes, it is the extracardiac comorbidities that are integral in disease progression and actively contribute to the syndrome of HFpEF (4). Although there are several shared comorbidities between patients with heart failure with reduced ejection fraction (HFrEF) and patients with HFpEF, the higher burden of a subset of comorbidities associated with HFpEF results in a higher risk of mortality (5). Within the growing number of cardiac and noncardiac comorbidities, the most common risk factors and/or comorbidities associated with HFpEF are age, female sex, hypertension, renal impairment, diabetes, and obesity (5).

Currently, the pathophysiological mechanisms involved in disease progression of HFpEF have yet to be clearly defined due primarily to the lack of

robust and translationally relevant animal models. The multiple phenotypes in HFpEF have proven difficult to recapitulate in an animal model. Typically, a single organ-single stressor approach is usually favored when developing animal models, which makes the multiple comorbidities associated with HFpEF difficult to mimic in the laboratory (4). One rodent model that has overcome this limitation and has shown to recapitulate several comorbidities through genetic selection is the ZSF-1 obese rat. The ZSF-1 rat model, which crosses the spontaneous hypertensive heart failure rat with a Zucker diabetic fatty rat, provides an overlapping genetic phenotype that predisposes the animals to hypertension and metabolic syndrome, 2 major prerequisites for the development of HFpEF (6). Several laboratories have demonstrated clinically relevant abnormalities in these animals that parallel human HFpEF (6,7). Various species and models have been used to model concentric LV hypertrophy, a hallmark of HFpEF, although none perfectly resembles the complex myocardial milieu seen with HFpEF. The hypertrophic, fibrotic, and impaired relaxation phenotype has been successfully modeled in dogs by repeated coronary microembolization (8) and in aged hypertensive dogs by renal wrapping (9). However,

From the ^aCardiovascular Center of Excellence, School of Medicine, Louisiana State University Health Science Center, New Orleans, Louisiana, USA; ^bDepartment of Pharmacology and Experimental Therapeutics, School of Medicine, Louisiana State University Health Science Center, New Orleans, Louisiana, USA; ^cDepartment of Animal Care, Louisiana State University Health Science Center, New Orleans, Louisiana, USA; ^dCardiovascular Institute, Department of Medicine, Perelman School of Medicine, University of Pennsylvania, Philadelphia, Pennsylvania, USA; and the ^eDepartment of Cardiology, Heart and Vascular Institute, Ochsner Medical Center, New Orleans, Louisiana, USA. Daniel Burkhoff, MD, served as Guest Editor for this paper. Michael R. Bristow, PhD, MD served as Guest Editor-in-Chief for this paper.

The authors attest they are in compliance with human studies committees and animal welfare regulations of the authors' institutions and Food and Drug Administration guidelines, including patient consent where appropriate. For more information, visit the [Author Center](#).

due to societal intolerance for canine experimentation and a growing number of phenotypically selective breeding and genetically modified pigs available, swine represent a more suitable large animal for HFpEF model development.

Swine models of HFpEF have been described with varying success using the most prominent of the comorbidities—hypertension, obesity, and diabetes mellitus generated typically as a single insult or as a 2-hit approach. Models that use hypertension as the sole driver of HFpEF pathophysiology include those that focus hypertension directly to the myocardium by mechanical manipulations to facilitate pressure overload LV hypertrophy. Devices that constrict the aorta with bands (10,11), cuffs (12,13), and stents (14), mitral regurgitation valve chordae rupture (15), and renal artery stenosis combined with ventricular pacing (16) all result in increased myocardial mass, stiffness, and fibrosis; however, the absence of multiorgan pathogenic effects significantly limits their clinical applicability. In contrast, pharmacological approaches to induce LV hypertrophy in swine through systemic hypertension by vasopressor (17–19) lack the severity to meaningfully affect cardiac function and fail to demonstrate overt heart failure at rest. In addition, efforts to incorporate obesity and diabetic comorbidities have been performed through Western diets (WD) high in fat, fructose, and salt, either alone or in combination with additional stressors in healthy swine (19–22), as well as strains predisposed to exhibit metabolic syndrome (23,24), and yet these models have failed to faithfully mimic the human HFpEF condition.

Unlike humans, many wild-type animal strains are highly resistant to diabetes, hypertension, atherosclerosis, and fail to exhibit cardiovascular diseases following prolonged exposure to risk factors (25–27). Using animals predisposed to cardiovascular disease provides an optimal background on which exposure to a WD and hypertension will ultimately induce HFpEF. Göttingen miniswine, bred principally for small size and ease of handling in a laboratory setting, were developed by crossbreeding the Vietnamese, Hormel, and German improved Landrace swine (28). The Göttingen miniswine are well described in relation to glucose metabolism and obesity, with a propensity to develop various aspects of the metabolic syndrome, including obesity, insulin resistance, and glucose intolerance when fed various high fat, WDs (28–30). The Göttingen miniswine also exhibit a propensity for development of dyslipidemia, vascular disease, and atherosclerosis (29). Although diabetes and obesity are crucial contributing comorbidities,

hypertension is critical in driving the pathophysiological HFpEF phenotype of concentric hypertrophic LV remodeling, myocardial fibrosis, and impaired ventricular relaxation.

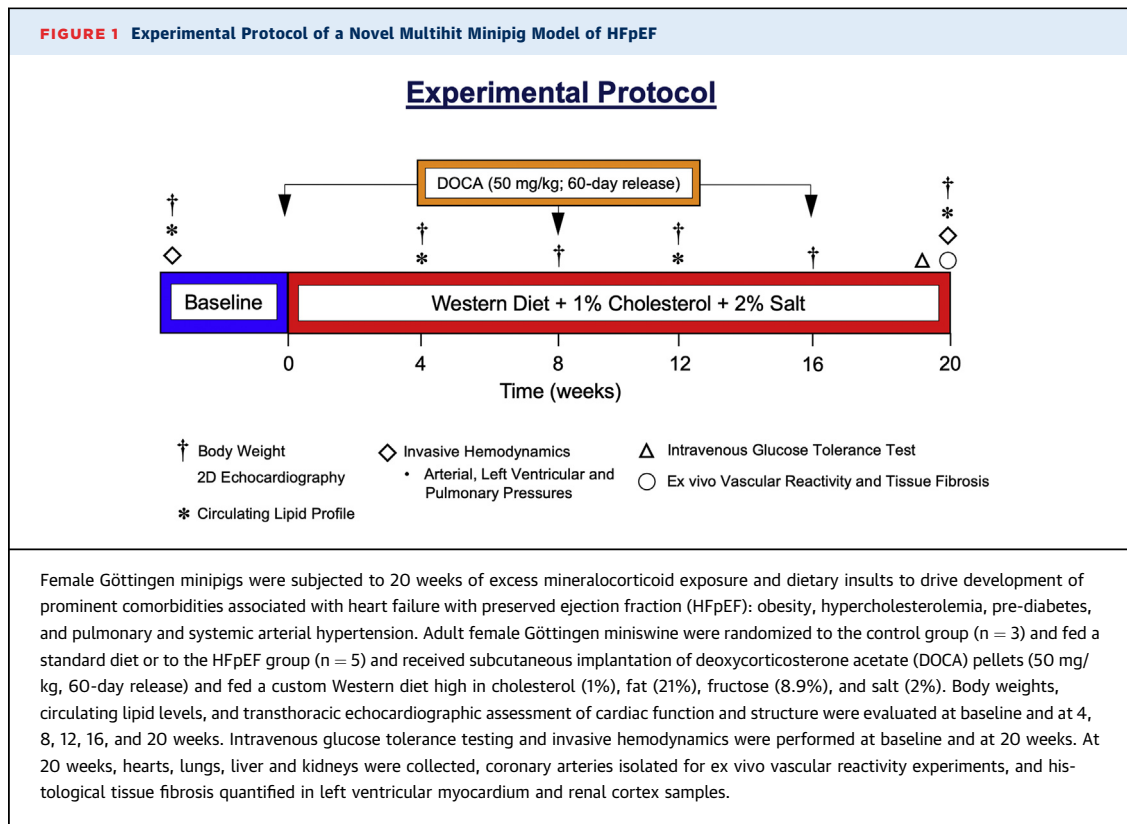
Using a multiplicity minimally invasive approach, we endeavored to create a clinically relevant miniswine model that combines 3 common comorbidities (metabolic syndrome, hypertension, female sex) that contribute to the complex pathophysiology of human HFpEF. Superimposing systemic hypertension using deoxycorticosterone acetate (DOCA) onto diet-induced obesity and a pre-diabetic phenotype in female Göttingen miniswine results in a novel animal model that exhibits the full spectrum of comorbidities and multiorgan involvement associated with HFpEF disease progression.

METHODS

EXPERIMENTAL DESIGN. All animal experiments were performed in accordance with the Guide for the Care and Use of Laboratory Animals, the Public Health Service Policy on the Humane Care and Use of Laboratory Animals, and the Animal Welfare Act. Institutional Animal Care and Use Committee approval was obtained from the Louisiana State University Health Sciences Center-New Orleans before initiation of these experimental studies.

Fourteen-month-old intact female Göttingen minipigs (17 to 20 kg) were acquired (Marshall Bio-Resources, Rose, New York) and assigned to 2 groups: healthy control swine (n = 3) and WD + DOCA-induced HFpEF (n = 8). One HFpEF animal succumbed to sudden death of unknown causes at 9 weeks; 2 HFpEF animals that exhibited severe end-organ damage, lethargy, and poor overall health were humanely euthanized at 10 weeks; these animals were not included in the final data analysis. Adjustments to amounts of HFpEF diet and DOCA were implemented, with the final constituents detailed in the following. Final outcome measures in the HFpEF group were assessed in 5 animals.

The control group were fed a standard diet (8753, Teklad Miniswine Diet, Envigo, Indianapolis, Indiana; 2.3 kcal/g⁻¹; carbohydrate: 33%; protein: 16%; fat: 3.9%; cholesterol: 0% wt/wt; sodium chloride: 0.4%; 900 g/day), whereas the HFpEF group was fed 50/50 (wt/wt) mix of standard diet and a custom WD containing high levels of fat, fructose, cholesterol, and salt (9GZC TestDiet, St. Louis, Missouri: Ossabaw atherosclerotic diet type 5B4L with 4% total salt; 4.01 kcal/g⁻¹; carbohydrate: 39.9% [17.8% high-fructose corn syrup]; protein: 16.2%; fat: 40%; cholesterol:



2%; sodium cholate: 0.7%; 900 g/day). Animals were fed once per day, and water was provided. Minipigs in the HFpEF group received a subcutaneous DOCA depot (50 mg/kg, 200 mg pellets, 60-day release; Innovative Research of America, Sarasota, Florida). Altogether, Göttingen miniswine in the control group (n = 3) and in the HFpEF group (n = 5) were studied for a total of 20 weeks (Figure 1).

BLOOD COLLECTION. Venous blood samples were obtained from anesthetized animals at baseline and at 4, 8, 12, 16, and 20 weeks, processed for serum, snap frozen, and stored at -80°C . Total cholesterol (TC), low-density lipoprotein (LDL), and high-density lipoprotein (HDL) levels were measured (IDEXX Laboratories, Memphis, Tennessee).

TRANSTHORACIC ECHOCARDIOGRAPHY. At baseline and at 4, 8, 12, 16, and 20 weeks, transthoracic echocardiography (Vivid E9, M5S transducer, GE Healthcare, Wauwatosa, Wisconsin) was performed in miniswine under ketamine/xylazine induction anesthesia (15 1.5 mg/kg, intramuscularly) and then isoflurane anesthesia (1.5% in 100% oxygen) as maintenance. To ensure accurate and consistent image acquisition, diltiazem (0.25 mg/kg) was administered to reach a target heart rate of <90 beats/min

(31). LV volumes and EF were measured using 2-dimensional auto-EF. Auto-EF uses speckle tracing technology and Simpson's method to track the endocardium through systole and diastole (32). LV wall thickness at end-systole and end-diastole were measured from subcostal 2-dimensional B-mode images acquired at the level of the mitral valve leaflets, as previously described (32). Left atrial areas and fractional area of change were measured from subcostal 2-dimensional B-mode views (33).

Pulse-wave Doppler echocardiography, with a maximal corrected angle of 40 degrees, was used to assess transmitral inflow velocities during diastole at the level of the mitral valve orifice. The ratio of peak early (E) and late (A) transmitral velocities was calculated. Pulse-wave tissue Doppler imaging, with a maximal corrected angle of 40 degrees, was used to calculate tissue velocities during early ventricular filling (\dot{e}) at the mitral valve medial and lateral annulus. Medial and lateral ratios of early transmitral inflow and tissue velocity (E/\dot{e}) were calculated (33). All images were acquired by a single cardiovascular researcher (T.E.S.) experienced in miniswine echocardiography. Analysis were performed off-line in a blinded fashion (GE EchoPAC Software, Version 202, GE Healthcare, Wauwatosa, Wisconsin).

INVASIVE HEMODYNAMICS. Miniswine underwent invasive systemic, LV, and pulmonary hemodynamic measurements at baseline and at 20 weeks. Animals were sedated as previously described, intubated, ventilated, and maintained under methohexital (Brevital, 7.0 to 8.0 mg/kg/h, intravenously) as previously described (32,34,35). Electrocardiography, heart rate, respiration rate, oxygen saturation, arterial blood pressure, and body temperature were continuously monitored. Using a standard sterile technique, percutaneous femoral artery and vein sheath introducers were placed under ultrasound guidance (Vivid E9, ML6-15 transducer, GE Healthcare). Systemic arterial blood pressures (systolic blood pressure [SBP], diastolic blood pressure [DBP], mean arterial pressure) were obtained from femoral artery access and recorded on the TruWave Pressure Transducer (Edwards Lifesciences, Irvine, California). For LV hemodynamics, a solid-state, single-pressure catheter (Millar Instruments, Houston, Texas) was advanced through the ascending thoracic aorta via femoral artery access under fluoroscopic guidance (Optima CL232i, GE Healthcare) and subsequently placed in the LV chamber for recording of LV pressures. Steady-state data were recorded (PowerLab 8/35, ADInstruments, Colorado Springs, Colorado) under spontaneous heart rate for a minimum of 10 consecutive beats with the ventilator tidal volume set to zero to eliminate respiratory artifact. Right heart catheterization was performed with a Swan-Ganz catheter (Edwards Lifesciences) placed in the left branch of the pulmonary artery via femoral vein access. Central venous pressure, pulmonary artery systolic, diastolic, mean, and wedge pressure (pulmonary systolic pressure and pulmonary capillary wedge pressure [PCWP], respectively) were recorded (TruWave Pressure Transducer, Edwards Lifesciences). Pressure measurements were performed off-line in a blinded fashion (LabChart 8 Software, ADInstruments).

CENTRAL VENOUS LINE PLACEMENT AND INTRAVENOUS GLUCOSE TOLERANCE TESTING. For intravenous glucose tolerance test (IVGTT) serial blood sampling, minipigs were sedated, anesthetized using isoflurane as previously described, and an indwelling catheter (Hickman, C.R. Bard, Inc, Salt Lake City, Utah) surgically placed in the right jugular vein as previously described (34,35). Surgical complications with implantation of 1 indwelling catheter led to only 4 HFpEF animals undergoing the IVGTT. Animals recovered for 3 days before IVGTT. At 20 weeks, conscious, overnight fasted miniswine received an intravenous bolus of 50% glucose solution (0.5 g/kg

body weight, Animal Health International, Patterson, Colorado), and blood samples (3 ml) were collected at -5, 0, 2.5, 5, 10, 20, 30, 40, 50, and 60 min. Blood glucose levels were monitored (Contour Blood Glucose Monitoring System, Bayer Healthcare, Mishawaka, Indiana) and plasma insulin values were measured (Insulin ELISA, Mercodia, Winston-Salem, North Carolina).

EUTHANASIA. At 20 weeks, minipigs were sedated, intubated, and anesthetized as previously described. Heparin (300 U/kg intravenously) was administered and under deep anesthesia, minipigs were euthanized (potassium chloride, 40 mEq/kg intravenously; Hospira, Inc, Lake Forest, Illinois) in accordance with the 2013 Edition of the AVMA Guidelines for the Euthanasia of Animals.

EX VIVO CORONARY VASCULAR REACTIVITY. Hearts were excised, and the left anterior descending and left circumflex coronary arteries carefully dissected, cut into 3 to 5 mm rings, and mounted onto the tension apparatus within organ bath chambers (Radnoti, Glass Technology, Monrovia, California) with oxygenated Krebs buffer for isometric tension experiments as previously described (32,36). Briefly, left anterior descending and left circumflex coronary arterial rings were placed under 2 g of pre-load tension and allowed to stabilize for 60 to 90 min. Coronary arterial ring viability was assessed using 50 and 100 mM potassium chloride consecutively. Rings were washed, pre-contracted with prostaglandin ($\text{PGF}_{2\alpha}$, 30 μM), and endothelial-dependent relaxation concentration curves were generated using bradykinin (10^{-11} to 10^{-6} M) and substance P (10^{-12} to 10^{-8} M). Endothelial-independent relaxation concentration curves were generated using sodium nitroprusside (10^{-9} to 10^{-5} M). Maximal relaxation and half-maximal effective concentrations (EC_{50}) were calculated.

CIRCULATING BIOMARKERS OF CARDIOVASCULAR DISEASE RISK. To assess oxidative stress in our model, we measured 8-isoprostane levels in plasma from baseline and at 4, 12, and 20 weeks in all animals using an enzyme-linked immunoassay kit (Cayman Chemical Company, Ann Arbor, Michigan). Endothelin-1 has been well established as a marker of endothelial dysfunction (37). Circulating serum levels of endothelin-1 were measured at baseline and at 4, 12, and 20 weeks in all animals using an enzyme-linked immunoassay kit (Enzo Lifescience, Farmingdale, New York).

RNA ISOLATION AND POLYMERASE CHAIN REACTION ANALYSIS OF NATRIURETIC PEPTIDES. Real-time

quantitative polymerase chain reaction mRNA levels of LV expression of natriuretic peptides were assessed as previously described (32). Briefly, mRNA was isolated from LV tissue and gene expression of atrial natriuretic peptide and B-type natriuretic peptide.

FIBROSIS STAINING AND QUANTIFICATION. Heart, lung, liver, and kidney specimens were harvested, fixed in 10% neutral-buffered formalin, processed for paraffin embedding, sections cut (5 μ m), stained with Masson's trichrome, and photomicrographs acquired. LV, pulmonary, hepatic, and renal cortical fibrosis was quantified by calculating the percentage of total Masson's trichrome positive tissue (blue) over the total tissue area using Image J software (National Institutes of Health, Bethesda, Maryland). Hepatic lobule area was quantified by identification of the central vein and the portal triads along the perimeter with an outline drawn around the perimeter and through the portal triads to acquire hepatic lobule area.

STATISTICAL ANALYSIS. All data are expressed as the mean \pm SEM. Statistical analyses were performed using Prism 6 (GraphPad Software, San Diego, California). A repeated mixed-effects model was performed for multiple comparisons between 2 groups over time with Sidak's post hoc test correction for multiple comparisons with a single pooled variance. A Student's unpaired Student's t-test was performed when comparing data from the 2 groups at a single time point. A 2-sided p value of <0.05 was considered statistically significant.

RESULTS

GÖTTINGEN MINIPIGS' ENHANCED SENSITIVITY TO MULTIPLE CARDIOVASCULAR DISEASE INSULTS.

Based on previous studies using WD-induced obesity in Göttingen minipigs (28,29), Göttingen miniswine were fed full rations of the custom WD containing 2% cholesterol and 4% sodium chloride (9GZC TestDiet). Because DOCA-induced hypertension had not been previously performed in Göttingen miniswine, we based our initial DOCA implantation regimen of 100 mg/kg, 90-day release pellets on reported published data using Landrace pigs (20). Following 4 weeks of WD diet and DOCA (100 mg/kg, 90 days), serum cholesterol levels increased 20-fold (data not shown) and Göttingen miniswine (n = 3) were returned to standard control diet. Although cholesterol levels improved when placed on standard diet, it appeared that the high levels of DOCA contributed to the moribund condition of the pigs, and consequently, 1 Göttingen minipig was lost due to sudden

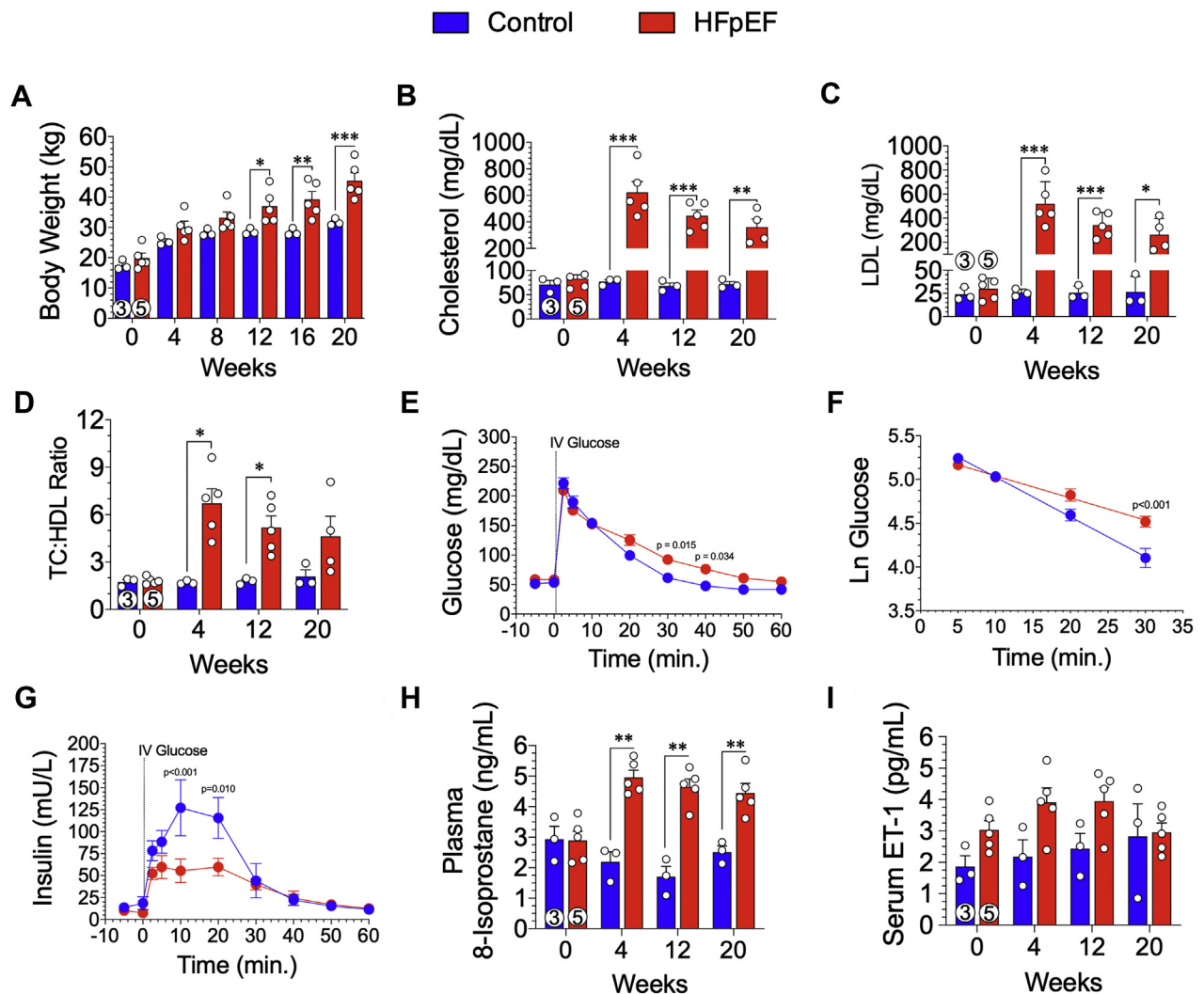
death, and the other 2 minipigs were humanely euthanized due to severe end-organ damage. As a result of the early mortalities, animals in the HFpEF group were subsequently fed a modified custom WD (50/50 wt mix with standard control diet [HFpEF diet]) and implanted with DOCA at 50 mg/kg, 200 mg pellets, 60-day release.

GÖTTINGEN MINIPIGS EXHIBIT OBESITY AND HYPERCHOLESTEROLEMIA.

Minipigs fed the HFpEF diet for 20 weeks gained significant (p = 0.050) weight starting at 12 weeks compared with the control diet fed animals (Figure 2A). At 20 weeks, HFpEF animals weighed 45.4 ± 2.7 kg compared with the control animals (31.7 ± 0.7 kg; p < 0.001) (Figure 2A). To confirm hypercholesterolemia, we performed serial blood draws and measured TC, LDL, and HDL. At 4 weeks, TC levels in the HFpEF animals was significantly (p < 0.001) increased compared with the control animals (623 ± 81.6 mg/dl vs. 77 ± 4.0 mg/dl, respectively) (Figure 2B). TC was significantly elevated throughout the 20-week study in HFpEF animals compared with the control animals (p = 0.003) (Figure 2B). As shown in Figure 2C, circulating LDL cholesterol levels exceeded 200 mg/dl during the study and were significantly elevated (p < 0.001 at 4 and 12 weeks; p = 0.020 at 20 weeks) compared with control animals. The TC/HDL ratio, a clinical index and independent risk predictor of heart disease was calculated (Figure 2D). At 4 and 12 weeks, the TC/HDL ratio was significantly (p = 0.021 and p = 0.034, respectively) elevated in HFpEF animals compared with control animals, although it was not significant at the 20-week timepoint.

ALTERED GLUCOSE METABOLISM AND CIRCULATING INSULIN LEVELS IN RESPONSE TO IVGTT.

Minipigs underwent intravenous glucose tolerance testing at 20 weeks to determine systemic responsiveness towards a glucose metabolism (Figures 2E to 2G). Baseline fasting blood glucose and insulin levels were similar between control animals and HFpEF animals at 20 weeks. Following intravenous administration of 0.5 g/kg of glucose, circulating levels increased to >200 mg/dl in all animals. At 30 and 40 min, post-intravenous glucose administration, circulating levels were significantly higher in HFpEF animals compared with control animals (p = 0.015 and p = 0.034, respectively) (Figure 2E). When calculating the natural log of glucose over 5 to 30 min, there was a significant (p < 0.001) reduction in the clearance of glucose over time (Figure 2F). Basal insulin levels were not different between groups, and following intravenous glucose administration, circulating insulin was significantly blunted in the HFpEF group

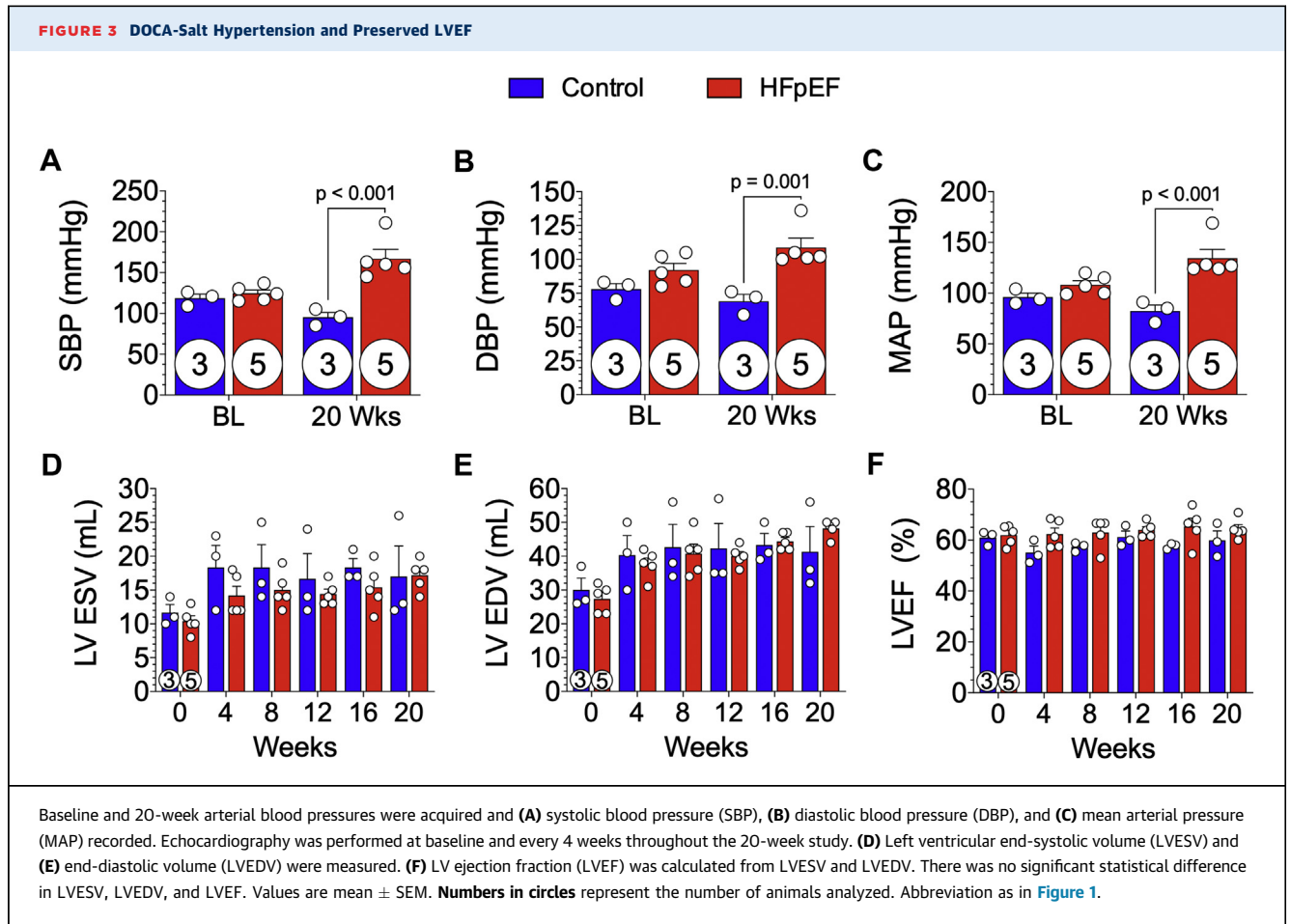
FIGURE 2 Development of Obesity, Dyslipidemia, Glucose Intolerance, and Risk Biomarkers of Cardiovascular Disease

(A) Body weights were obtained at baseline and every 4 weeks throughout the 20-week study. Lipid profiling was performed at baseline and at 4, 12, and 20 weeks. (B) Total cholesterol (TC), (C) low-density lipoprotein (LDL), and (D) ratio of TC to high-density lipoprotein (HDL) were measured. At 20 weeks, conscious intravenous (IV) glucose tolerance testing was performed in overnight fasted minipigs. (E) Glucose levels were measured from timed blood samples obtained over 60 min following IV glucose administration. (F) The natural log (Ln) of glucose was determined 5 to 30 min following IV glucose administration was calculated. (G) Insulin levels were measured from timed blood samples obtained over 60 min following IV glucose administration. (H) Circulating plasma 8-isoprostane levels were measured at baseline and at 4, 12, and 20 weeks. (I) Serum endothelin (ET)-1 levels were measured at baseline and at 4, 12, and 20 weeks. Values are mean \pm SEM; * $p < 0.05$; ** $p < 0.01$; *** $p < 0.001$, for significantly different versus control. Numbers in circles represent the number of animals analyzed. Abbreviation as in Figure 1.

between 10 and 30 min ($p < 0.001$ and $p = 0.010$, respectively) (Figure 2G).

Biomarkers of cardiovascular disease risk. Oxidative stress is a driving force of long-term abnormalities in cardiovascular disease. 8-Isoprostane was measured in the plasma in all animals at baseline and at 4, 12, and 20 weeks in the study (Figure 2H). At baseline, there was no significant difference between

groups. As early as 4 weeks and throughout the entire study, 8-isoprostane levels were significantly ($p \leq 0.009$) elevated in the HFpEF group compared with the control group (Figure 2H). Endothelin-1, a marker of endothelial dysfunction in cardiovascular disease, including coronary artery disease and peripheral artery disease, was measured at baseline and at 4, 12, and 20 weeks. Although elevated throughout the

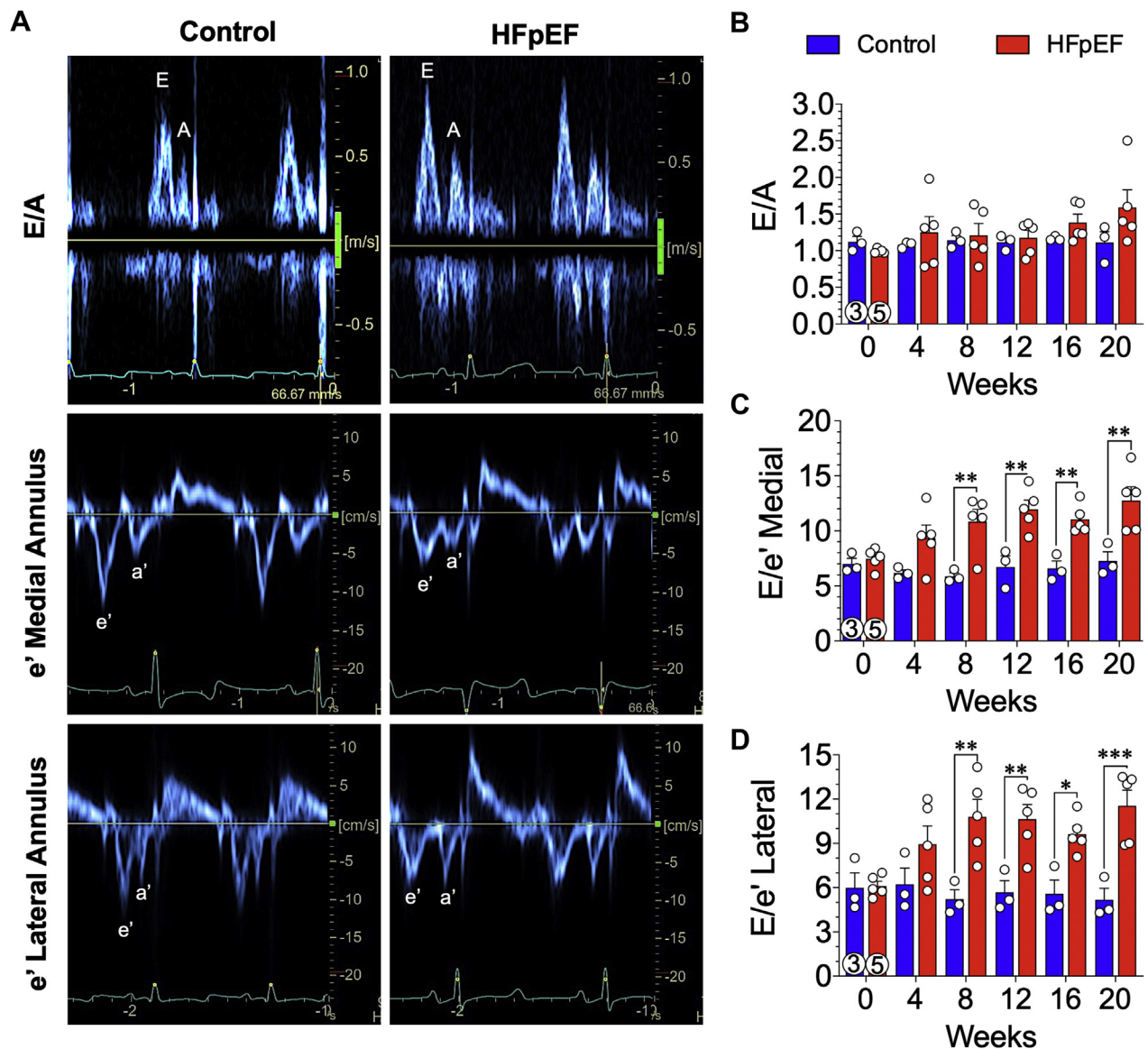


study at 4, 12, and 20 weeks in the HFpEF group compared with the control group, there was no statistical difference between the groups ($p = \text{NS}$) (Figure 2I).

DOCA- AND SALT-INDUCED HYPERTENSION. DOCA pellet implantation (50 mg/kg, 60-day release) and increased dietary salt intake in HFpEF miniswine resulted in significant elevations in systemic blood pressures at 20 weeks (Figure 3). Arterial invasive hemodynamic measurements were obtained at baseline and at 20 weeks. SBPs were similar at baseline but were significantly higher at 20 weeks in the HFpEF group compared with the control group (167 ± 11.4 mm Hg vs. 95 ± 5.8 mm Hg, respectively; $p < 0.001$) (Figure 3A). DBPs were not different at baseline but were significantly higher at 20 weeks in the HFpEF group compared with the control group (109 ± 6.9 mm Hg vs. 69 ± 5.1 mm Hg, respectively; $p = 0.001$) (Figure 3B). Mean arterial pressure at 20 weeks was significantly higher in HFpEF animals (134 ± 8.7 mm Hg vs. 82 ± 6.0 mm Hg [control animals]) (Figure 3C).

PRESERVED LV SYSTOLIC FUNCTION WITH PROGRESSIVE DIASTOLIC DYSFUNCTION. Echocardiograms acquired every 4 weeks revealed that systolic LV function was maintained over the 20-week study (Figures 3D to 3F). There were no significant differences in end-systolic or end-diastolic volumes between HFpEF and control minipigs (Figures 3D and 3E). LVEF was unchanged throughout the 20-week study in HFpEF and control minipigs (Figure 3F).

Diastolic function was assessed by measuring mitral valve inflow velocity using pulse-wave Doppler and tissue Doppler echocardiography of the medial and lateral mitral valve annulus (Figure 4). Representative images of mitral inflow velocities (top row) and tissue Doppler (bottom rows) from control and HFpEF minipigs at 20 weeks are shown (Figure 4). During the 20-week study, mitral valve inflow velocity (E/A ratio) was not significantly different between control and HFpEF minipigs (Figure 4B); however, the ratio of early inflow velocity (E) over tissue velocity (\dot{e}) was significantly elevated in the HFpEF minipigs

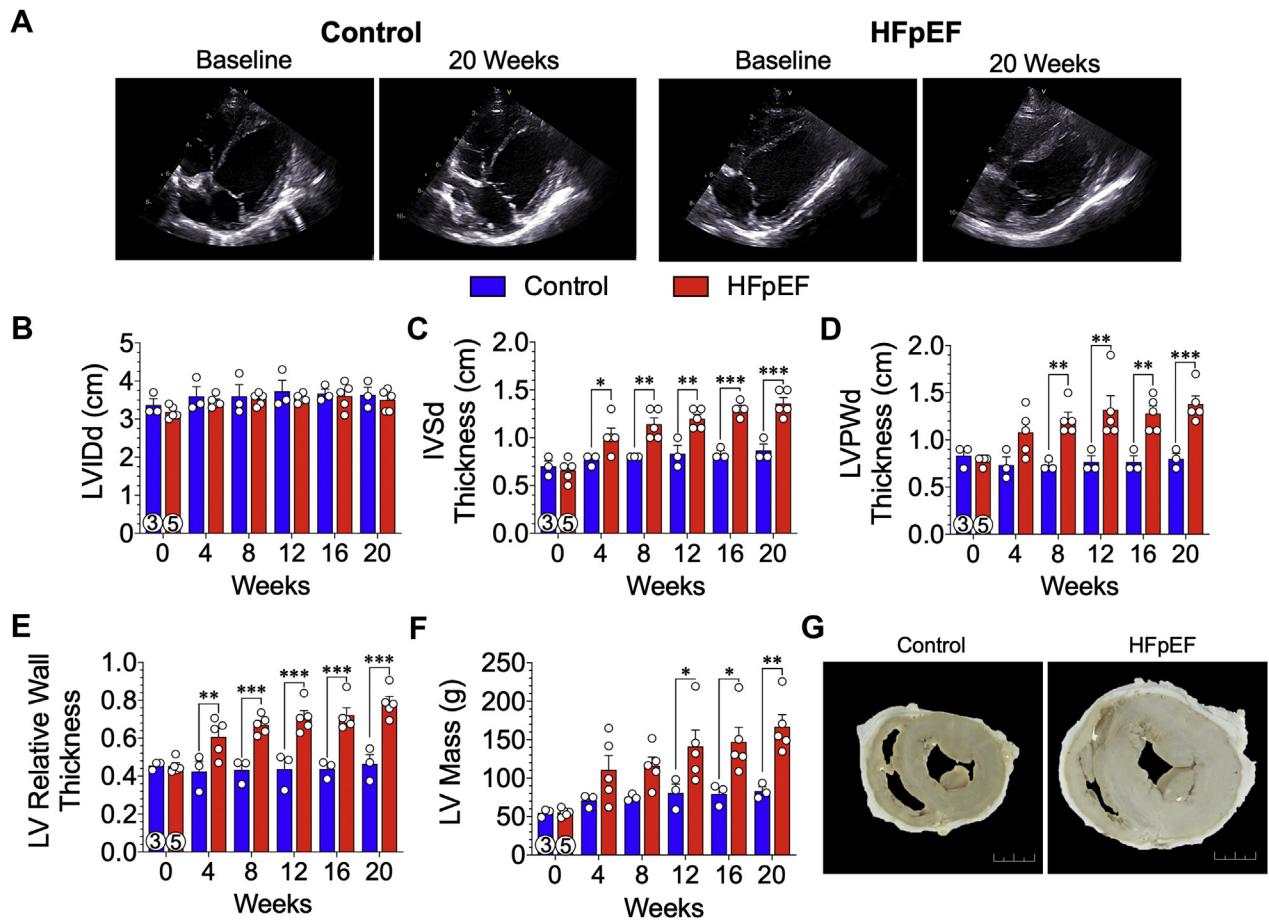
FIGURE 4 Increased E/é Ratio Indicative of LV Diastolic Dysfunction

Indicators of cardiac filling pressures were evaluated noninvasively at baseline and every 4 weeks throughout the 20-week study. Transmittal inflow velocity was measured by pulse-wave Doppler echocardiography, and mitral annular velocity was measured by pulse-wave tissue Doppler imaging. **(A)** Representative trace recordings of mitral inflow (E/A) and tissue Doppler medial and lateral mitral annular velocities (é) at 20 weeks from control and HFpEF minipigs. Peak early (E) and late atrial (A) diastolic transmittal flow velocity along with early (é) and late atrial (á) diastolic mitral annular velocity were noted. **(B)** Early-to-late diastolic transmittal flow velocity (E/A) ratios were not statistically different. The E to early diastolic mitral medial **(C)** and lateral **(D)** annular tissue velocity (E/é) ratios were also calculated. Values are mean \pm SEM; * $p < 0.05$; ** $p < 0.01$; *** $p < 0.001$ for significantly different versus control. **Numbers in circles** represent the number of animals analyzed. Abbreviation as in **Figure 1**.

starting at 8 weeks and remained elevated at all subsequent timepoints (**Figures 4C and 4D**). By 8 weeks, the medial E/é ratio (**Figure 4C**) was significantly elevated in HFpEF minipigs compared with control animals and was sustained over the course of the study (20 weeks: HFpEF: 12.8 ± 1.3 ;

control: 7.3 ± 0.8 ; $p = 0.002$). By 8 weeks, the lateral E/é ratio (**Figure 4D**) was significantly elevated in HFpEF minipigs compared with control animals and was sustained over the course of the study (20 weeks: HFpEF: 11.5 ± 1.1 ; control: 5.2 ± 0.8 ; $p < 0.001$).

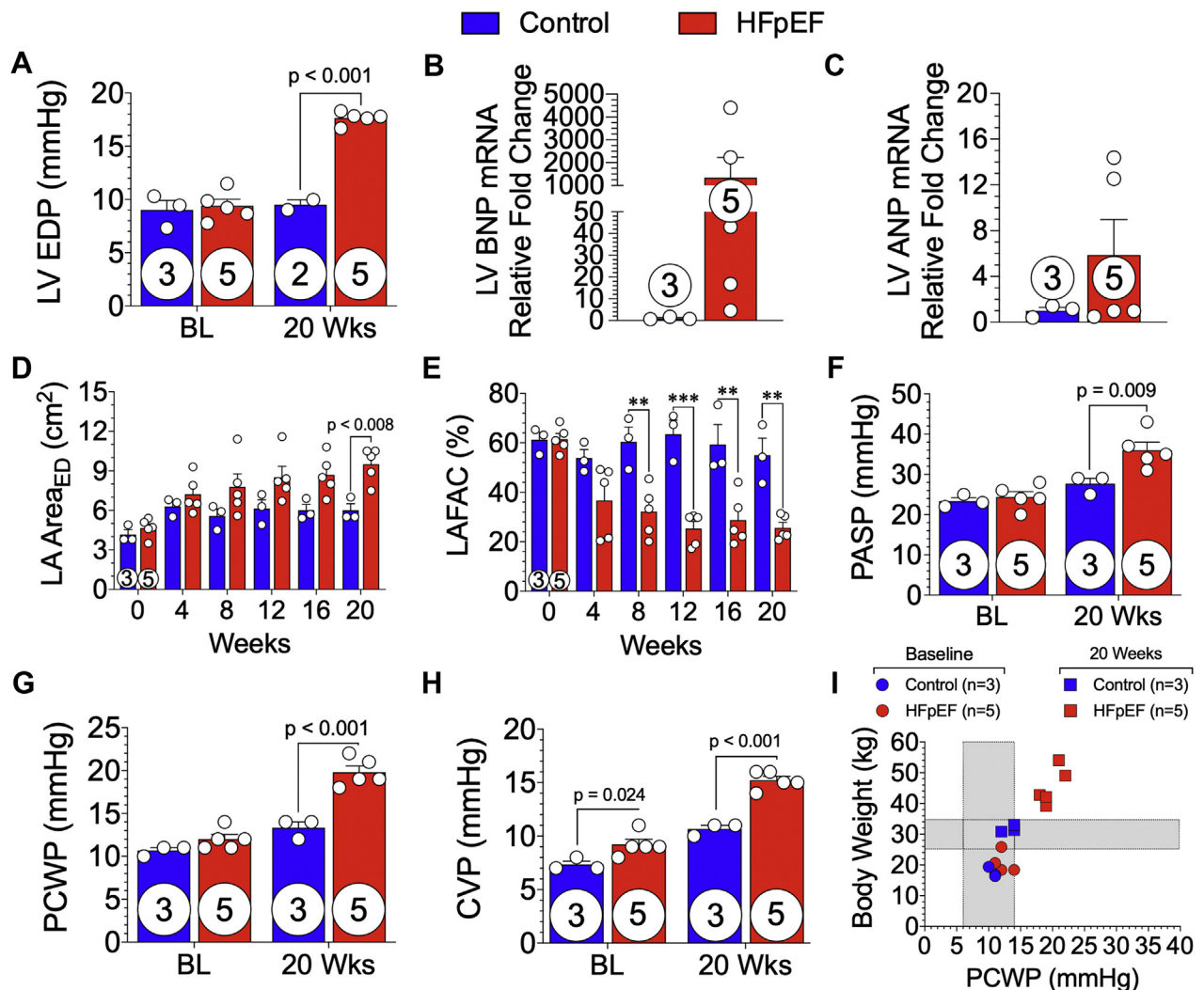
FIGURE 5 Pathophysiological Concentric Hypertrophy of the LV



(A) Representative transthoracic echocardiographic subcostal 2-dimensional B-mode images of the LV acquired at baseline and 20 weeks from control and HFpEF minipigs. (B) LV chamber internal diameter (LVID) were measured from images during end-diastole (d), which was not statistically different. (C) Thickness of the interventricular septum (IVS) and (D) LV posterior wall (LVPW) were measured from images during end-diastole (d). (E) LV relative wall thickness and (F) LV mass were derived using the end-diastolic linear measurements of the LVID, IVS, and LVPW measurements. (G) Representative photomicrographs of gross mid-papillary cross sections from a control heart and a HFpEF heart. Scale bar: 2 cm. Values are mean \pm SEM; * $p < 0.05$; ** $p < 0.01$; *** $p < 0.001$, for significantly different versus control. Numbers in circles represent the number of animals analyzed. Abbreviations as in Figures 1 and 3.

INCREASED LV WALL THICKNESS AND CONCENTRIC HYPERTROPHY. Serial echocardiographic assessment of LV structure showed progressive and significant thickening of the LV walls in HFpEF miniswine (Figure 5). In Figure 5A, representative subcostal 2-dimensional B-mode images of control (left panels) and HFpEF (right panels) hearts at baseline and 20 weeks are shown. LV chamber dimensions did not change between groups throughout the study (Figure 5B). As early as 4 weeks, there was a significant and sustained ($p = 0.036$) increase in end-diastolic intraventricular septal wall thickness (Figure 5C) in HFpEF minipigs compared with control animals (20 weeks: 1.36 ± 0.06 cm vs. 0.87 ± 0.07 cm,

respectively; $p < 0.001$). As shown in Figure 5D, there was a significant and sustained increase in LV end-diastolic posterior wall thickness starting at 8 weeks ($p = 0.005$). Baseline relative wall thicknesses (Figure 5E) were similar between groups; however, beginning at 4 weeks, there was a significant increase in relative wall thickness in the HFpEF minipigs compared with control animals (0.61 ± 0.04 cm vs. 0.42 ± 0.06 cm, respectively; $p = 0.009$) that continued to increase over the course of the study (20 weeks: HFpEF: 0.79 ± 0.03 cm; control: 0.46 ± 0.05 cm; $p < 0.001$). Calculated echocardiographic LV mass (Figure 5F) was similar between groups at baseline and at 4 and 8 weeks. At 12 weeks, there was

FIGURE 6 Elevated LV Filling Pressures Promote Left Atrial Dysfunction, Leading to Combined Pre- and Post-Capillary Pulmonary Hypertension

Invasive LV hemodynamic measurements were acquired at baseline (BL) and 20 weeks from control and HFpEF minipigs. **(A)** LV end-diastolic pressure (LVEDP) was calculated. **(B)** B-type natriuretic peptide (BNP) and **(C)** atrial natriuretic peptide (ANP) mRNA expression of LV tissue. **(D)** Left atrial (LA) area at end-diastole (ED) and **(E)** LA fractional area change (LAFAC) were measured from subcostal 2-dimensional B-mode echocardiographic images acquired at baseline and every 4 weeks during the 20-week study from control and HFpEF minipigs. **(F)** Pulmonary artery systolic (PASP) and **(G)** pulmonary capillary wedge pressure (PCWP) and **(H)** central venous pressure (CVP) were measured at baseline and 20 weeks in control and HFpEF minipigs. **(I)** The relationship of body weight to PCWP at baseline and 20 weeks was plotted. Values are mean \pm SEM; **p < 0.01; ***p < 0.001, for significantly different versus control. **Numbers in circles** represent the number of animals analyzed. Abbreviations as in [Figures 1 and 3](#).

a significant increase in LV mass in HFpEF minipigs compared with control animals (141 ± 21 g vs. 81 ± 12 g, respectively; $p = 0.052$), and at the 20-week endpoint, estimation of LV mass in the HFpEF group was 167 ± 16 g ($p = 0.003$ vs. control animals). In [Figure 5G](#), representative photomicrographs of mid-papillary cross sections of the myocardium from a control and HFpEF heart demonstrate a clear difference in morphometry of the heart.

ELEVATED LV FILLING PRESSURES WITH LEFT ATRIAL REMODELING AND DYSFUNCTION. In the HFpEF minipigs, we observed a significant elevation in LV pressures coupled with adverse remodeling and function of the left atria ([Figure 6](#)). LV pressures were acquired in all animals at baseline and in all HFpEF and 2 control minipigs at 20 weeks. In [Figure 6A](#), LV end-diastolic pressure was significantly ($p < 0.001$) increased in HFpEF animals (17.7 ± 0.3 mm Hg) at the

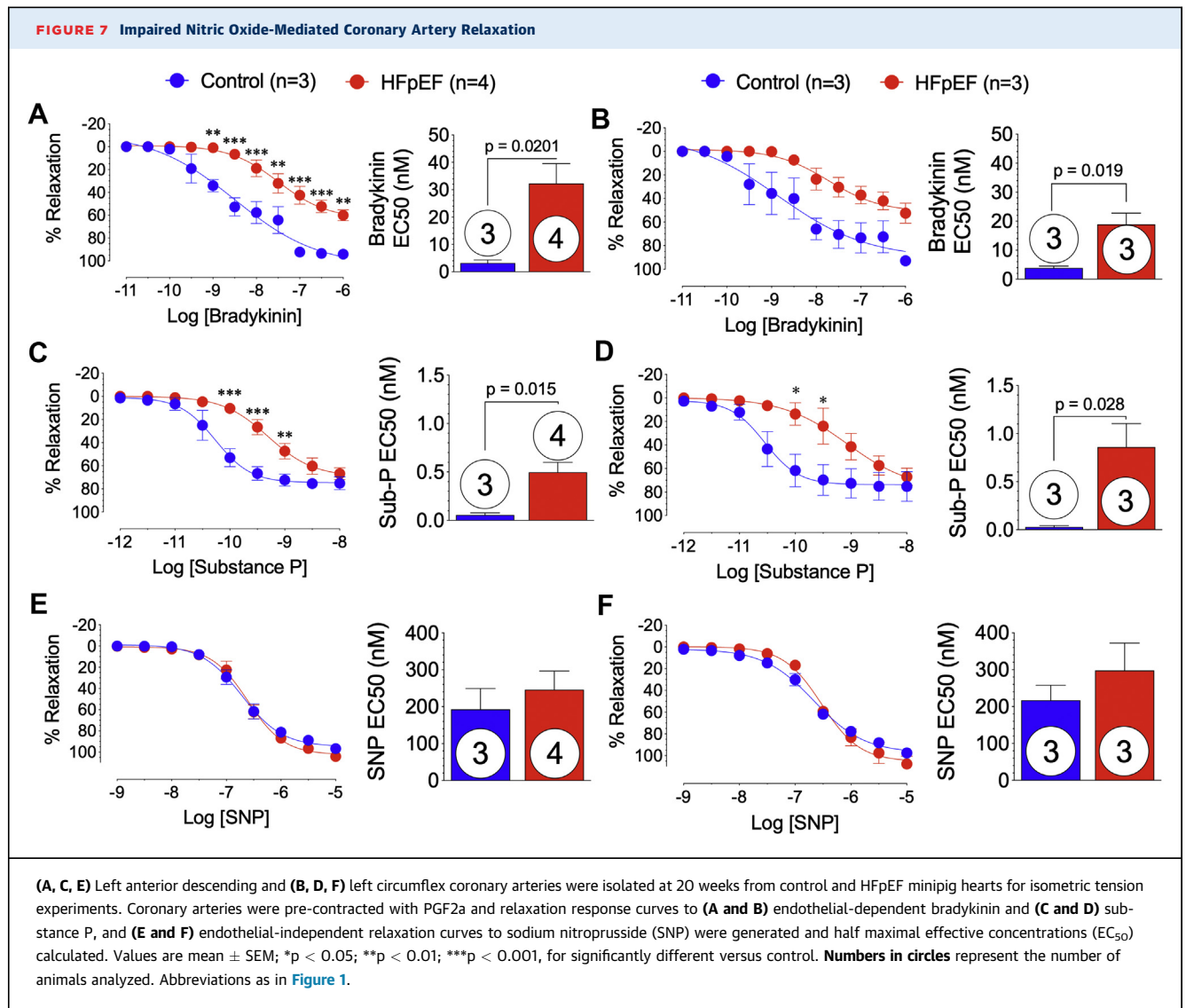
20-week timepoint and unchanged in control animals (9.0 ± 0.9 mm Hg [baseline]; 9.5 ± 0.5 mm Hg [20 weeks]). In **Figure 6B**, LV mRNA expression of B-type natriuretic peptide was elevated by >4.5-fold in every animal in the HFpEF group compared with that of control animals. However, due to variability in the HFpEF group and small sample size, B-type natriuretic peptide expression levels did not demonstrate statistical significance. LV atrial natriuretic peptide expression was not statistically different between groups (**Figure 6C**). **Figure 6D** demonstrates progressive remodeling of the left atria as measured using echocardiography of left atrial area at end-diastole. The mean left atrial area (**Figure 6D**) at 20 weeks was 9.5 ± 0.6 cm² in HFpEF minipigs compared with 6.0 ± 0.5 cm² in control animals ($p = 0.008$). The left atrial fractional area of change was significantly reduced in HFpEF minipigs as early as 8 weeks ($p = 0.002$) and continued to deteriorate over time compared with control animals (**Figure 6E**).

PRE- AND POST-CAPILLARY PULMONARY HYPERTENSION. Right heart catheterization was performed at baseline and 20 weeks to assess pulmonary pressures (**Figure 6**). At baseline, there were no significant differences ($p = \text{NS}$) in pulmonary systolic (**Figure 6F**) and wedge pressures (**Figure 6G**) between control and HFpEF groups. At 20 weeks, pre-capillary pulmonary arterial hypertension was observed, in which there was a significant increase in pulmonary systolic pressure (**Figure 6F**) in HFpEF minipigs compared with control animals (36.0 ± 2.0 mm Hg vs. 24.4 ± 1.3 mm Hg, respectively; $p = 0.009$). As shown in **Figure 6G**, PCWP was significantly elevated ($p < 0.001$) at 20 weeks in HFpEF minipigs compared with control animals (19.8 ± 0.7 mm Hg vs. 12.0 ± 0.6 mm Hg, respectively). There was a significant ($p < 0.001$) increase in central venous pressure (**Figure 6H**) at 20 weeks in HFpEF minipigs (15.2 ± 0.4 mm Hg). In **Figure 6I**, we observed a positive correlation in body weight and PCWP in HFpEF minipigs.

IMPAIRED CORONARY ARTERY ENDOTHELIAL FUNCTION. In the setting HFpEF, there is profound coronary artery dysfunction manifested by impaired relaxation to endothelial-dependent agonists (1). At 20 weeks, left anterior descending and left circumflex coronary arteries were isolated from control and HFpEF Göttingen minipig hearts. Ex vivo vasodilatory responses to endothelial-dependent (bradykinin and substance P) and -independent (sodium nitroprusside) agonists were shown (**Figure 7**). Left

anterior descending coronary arteries from HFpEF minipigs demonstrated significant ($p \leq 0.001$) attenuation of relaxation to bradykinin (10^{-9} to 10^{-6} M) and significantly greater EC₅₀ compared with control animals ($p = 0.020$) (**Figure 7A**). Although relaxation response curves to bradykinin were similar, the EC₅₀ was significantly ($p = 0.019$) greater in left circumflex coronary arteries isolated from HFpEF minipigs compared with control animals (**Figure 7B**). Coronary vasodilatory responses to substance P (**Figures 7C and 7D**) were significantly attenuated at 10^{-10} to 10^{-9} M concentrations in the left anterior descending ($p < 0.001$ and $p = 0.016$, respectively) and left circumflex ($p < 0.05$) arteries and had significantly greater EC₅₀ ($p = 0.015$ and $p = 0.028$, respectively) from HFpEF minipigs compared with control animals. Endothelial-independent relaxation responses to sodium nitroprusside were similar in left anterior descending and left circumflex coronary arteries isolated from control and HFpEF minipigs (**Figures 7E and 7F**).

MULTIORGAN HISTOPATHOLOGY WITH INCREASED LV MYOCARDIAL AND RENAL FIBROSIS. In HFpEF minipigs, representative photomicrographs of LV Masson's trichrome stain demonstrated increased myocardial fibrosis associated with interstitial lipid deposition within the mid-myocardium (**Figure 8A**). When fibrosis was quantified as a percentage of total tissue area, there was a significant ($p = 0.003$) increase in myocardial fibrosis in HFpEF minipig hearts compared with control animals (**Figure 8B**). Representative photomicrographs of Masson's trichrome stained lung tissue from control and HFpEF minipigs showed a difference in aveolar structure, as well as accumulation of cell infiltrate around pulmonary vasculature and airways (**Figure 8C**). When total pulmonary fibrosis was quantified as a percentage of total tissue area, there was no significant difference (**Figure 8D**). Representative photomicrographs of liver Masson's trichrome stain demonstrated interlobular fibrosis (**Figure 8E**); however, when quantified, there was no significant difference between groups (**Figure 8F**). Representative kidney cortical tissue samples from control and HFpEF minipigs showed an increase in both glomerular and tubular fibrosis compared with control animals (**Figure 8G**). Total renal fibrosis, quantified as a percentage of Masson's trichrome stained tissue to total tissue area (**Figure 8H**) was significantly ($p = 0.022$) increased in HFpEF minipigs compared with control animals ($42 \pm 3\%$ vs. $27 \pm 3\%$, respectively).



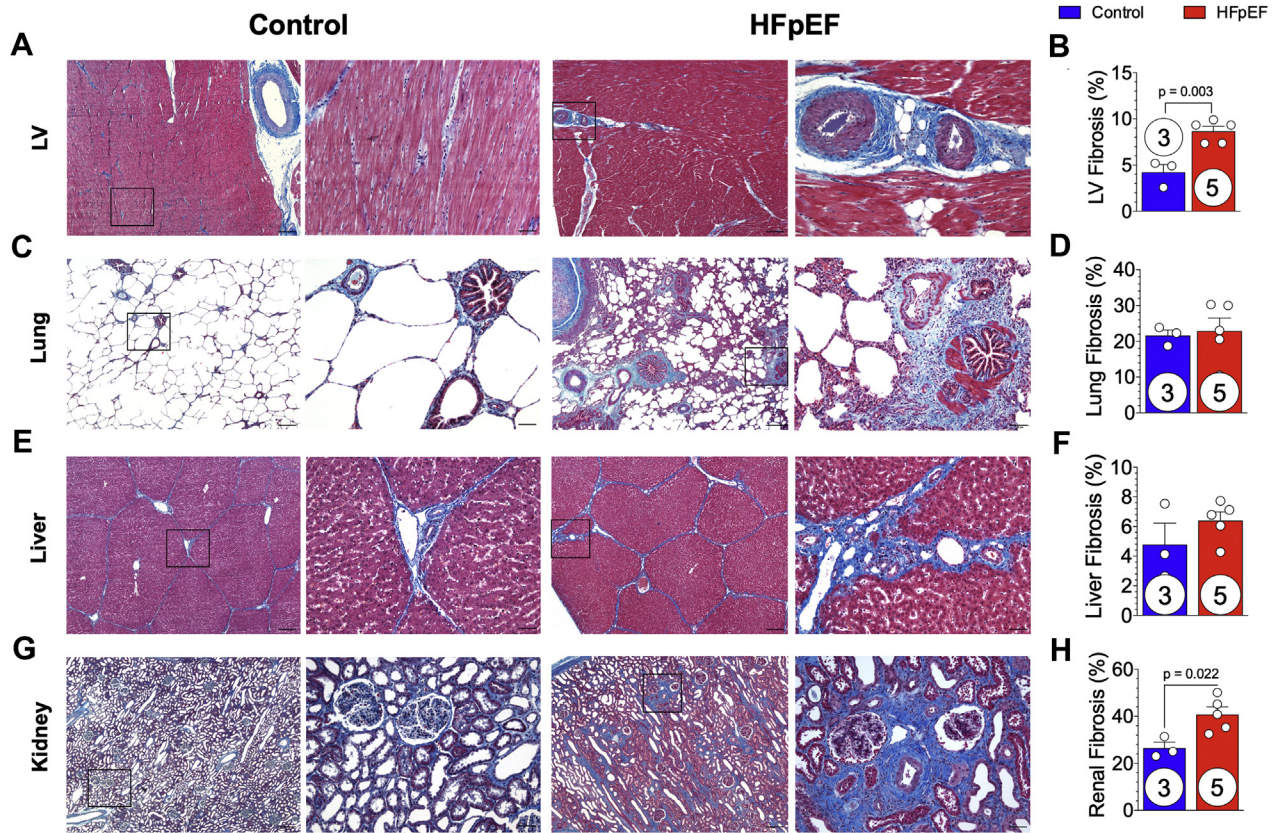
DISCUSSION

In this study, we reported on a novel large animal model of HFpEF induced through dietary and long-term mineralocorticoid administration using a well-established minipig breed with known susceptibilities toward obesity, metabolic syndrome, and atherosclerosis. Severe LV diastolic dysfunction was evidenced by significant elevations in end-diastolic pressure, diastolic early filling velocities (E/\dot{e}), coupled with profound myocardial hypertrophy and fibrosis during which EF was preserved. We observed significant vascular injury and dysfunction evidenced by pulmonary and systemic hypertension, as well as impaired coronary artery

endothelial-dependent vasorelaxation responses in vitro. In addition to the cardiac pathology, this HFpEF model encompassed impairments across multiple organ systems, including the pancreas, liver, and kidney, as exhibited by significant blunting of glucose and insulin handling, elevated circulating cholesterol levels, and increased renal fibrosis.

The combination of established methods of DOCA-salt induced hypertension and WD metabolic syndrome have not been previously performed in Göttingen miniswine. Our results described a unique miniswine translational animal model that exhibited the spectrum of multiorgan pathophysiology characteristic of human HFpEF.

FIGURE 8 Multiorgan Histopathology and Fibrosis



At 20 weeks, hearts, lungs, liver, and kidneys were collected from control and HFpEF minipigs. Tissue samples were processed for histological Masson's trichrome staining, micrographs were acquired, and the amount of fibrosis quantified. Representative low (4×) and high (20×) magnification images of (A) LV myocardial tissue, (C) lung tissue, (E) liver tissue, and (G) renal cortical tissue samples from control and HFpEF minipigs are shown. Percentage of fibrosis area of Masson's trichrome-stained (B) LV myocardial, (D) lung, (F) liver, and (H) renal cortical tissue sections were quantified. Scale bars: 4×, 200 μm; 20×, 50 μm. Values are mean ± SEM. Numbers in circles represent the number of animals analyzed. Abbreviations as in Figures 1 and 3.

There is universal agreement that the lack of suitable preclinical animal models of HFpEF is among the largest roadblocks to advancing our understanding of HFpEF and developing novel therapies to treat patients with HFpEF. Most of the previous described HFpEF models consisted of cardiac pressure overload to induce LV concentric hypertrophy and diastolic dysfunction, but these models failed to fully capture the characteristics of human HFpEF and have not proven to be reliable for preclinical evaluation of potentially new therapeutic targets (38). Purported animal models of HFpEF exhibited select features of human condition and did not truly reflect the full spectrum of pathological phenotypes observed in patients with HFpEF (39). To our knowledge, the Göttingen minipig DOCA-salt and WD model

described here is the only large animal model to date that exhibited definite evidence of advanced, severe HFpEF. Clinically, diagnostic confirmation of HFpEF requires either elevated LV filling pressures at rest (LV end-diastolic pressure >16 mm Hg) or an elevated mean capillary wedge pressure at rest (PCWP p > 15 mm Hg) in the presence of normal systolic LV function (LVEF >50%) (40-43). As we demonstrated, the Göttingen DOCA-salt and WD model exhibited elevated LV filling pressures at rest (LV end-diastolic pressure: 17.7 ± 0.3 mm Hg) and elevated mean capillary wedge pressure at rest (PCWP: 19.8 ± 0.7 mm Hg) in the presence of normal systolic LV function (LVEF: 64.3 ± 1.8%). Furthermore, this model was representative of advanced HFpEF because LV filling pressures were elevated at rest,

whereas an earlier stage of HFpEF is characterized by LV pressure increases observed only during exercise (22). Several other swine models established comorbid-laden models attempting to mimic HFpEF (24,44); however, they did not demonstrate the clinical endpoints necessary for classification of HFpEF, specifically the noninvasive diastolic echocardiographic measurement of E/e' and the invasive hemodynamic measurements of elevated LV end-diastolic pressure or elevated PCWP (42,45).

It is well recognized that diastolic dysfunction by itself is not enough to produce HFpEF; additional cardiac and extracardiac abnormalities involving multiple organs are critical in capturing the heterogeneity of HFpEF pathophysiology. In the present study, we used a systemic, multiorgan approach by subjecting the whole animal to hypertension and a high-fat, high-salt WD that resulted in a spectrum of pathologies involving a number of organs. Moreover, the diverse spectrum of HFpEF pathologies encompassed in this Göttingen minipig HFpEF model was ideally suited for evaluating the degree to which each of the organ systems was altered and the relative impact of each comorbidity on the overall clinical condition (38).

Until now, absence of an animal model that comprehensively exhibited the heterogeneity of the HFpEF clinical condition has forced the field to compromise and reluctantly accept animal models that only recapitulated partial HFpEF phenotypes (38). Developing a disease phenotypically characterized by multi-comorbidities and multiorgan dysfunction is further complicated, in that each comorbidity is in itself a standalone multifaceted disease with distinct phenotypes driven by a combination of different genetic, dietary, and environmental factors. The challenge, similar to that observed among patients with HFpEF, is that with a higher burden of comorbidities comes a higher risk of mortality (5). High mortality rates have also been reported in many preclinical HF swine models that have been induced by multiple insults to mimic the multiple comorbidities (21), which occurred during our initial development of the model. Early in model development, we failed to recognize the unique impact of the Göttingen minipig strain on disease progression. Reliance on previously reported doses and duration of DOCA administration using younger Landrace swine (20,46,47) proved catastrophic, causing circulating lipid levels to soar and systemic and LV pressures to skyrocket, which resulted in rapid end-organ damage and circulatory collapse.

The "too much, too fast" is certainly not the clinical scenario because aging in the setting of long-standing hypertension and metabolic syndrome are critically important contributors to the HFpEF condition. Göttingen miniswine are commonly used as models of obesity, metabolic syndrome, and hypercholesterolemia (28-30). These comorbidities manifest as early as after 2 to 5 weeks of a high-cholesterol and/or high-fat diet in comparison to most other metabolic syndrome swine models, including the Ossabaw strain in which features of this disorder require 3 to 6 months of diet to appear. The applicability of using the Göttingen minipig strain over other swine strains for modeling human HFpEF is further evidenced by its genetic diversity. It has been suggested that similar to human HFpEF, the use of outbred murine colonies could contribute to a better experimental setting because, in contrast, the use of inbred strains represents limited genetic diversity and might not reflect the responses generated in a diverse human population (1,48). Although the Ossabaw strain encompasses descendants of minipigs brought from Spain, their isolation on Ossabaw Island has resulted in a breed that has lived in relative genetic isolation for centuries (49). Göttingen minipig genetic diversity stems from the crossbreeding of the Minnesota minipig, the Vietnamese pot-bellied pig, and the German Landrace pig (28). Lastly, and equally important when developing animal models designed to assess therapeutic efficacy of novel interventions, body size often limits the type of study. The major advantage of rodents is the fact that pharmacological studies require lesser amounts of test agents, and rodents are suitable for genetic manipulations to create transgenic models that aid in the elucidation of pathological mechanisms. However, because of the current lack of effective treatments for HFpEF coupled with the multifactorial nature of HFpEF pathophysiology, devices and technologies are also being explored, which necessitates animals large enough as would be used in patients with HFpEF. The size of the Göttingen minipig makes this strain more suitable for HFpEF studies because they are the smallest of the swine breeds, which facilitates pharmacological studies while at the same time being large enough for device testing.

STUDY LIMITATIONS. The low number of animals was perhaps a limitation of the present study; however, statistical significance was achieved in all of the key diagnostic functional, structural, and histological criteria for definitive confirmation of advanced HFpEF. Before embarking on an exhaustive comprehensive characterization of a HFpEF model, we

sought to establish and confirm that the Göttingen minipig model presented in this study accurately and appropriately recapitulated all of the comorbidity complexities characteristic of the human HFpEF condition. Physiological functional stress exercise capacity testing with complimentary molecular mechanistic investigations into the role of inflammation, cGMP/PKG signaling, and titin-actin interactions are clearly warranted and will only be meaningful and clinically translatable if we start with the correct animal model preclinical platform.

CONCLUSIONS

In summary, our results demonstrated that the combination of DOCA-salt induced hypertension and a high-salt, WD-induced metabolic syndrome in the Göttingen minipig strain exhibited a full spectrum of HFpEF phenotypes. This novel large animal model of HFpEF represents an important preclinical research tool that will drive future studies to identify key molecular mechanisms and evaluate potential therapeutics for HFpEF. The Göttingen minipig HFpEF model also permits a multidimensional phenotypic readout of therapeutic efficacy (i.e., antihypertensive effects, obesity, and metabolic syndrome effects), which could help identify patient subgroups most likely to benefit from a specific intervention.

FUNDING SUPPORT AND AUTHOR DISCLOSURES

Dr. Kelly is supported in part by the National Institutes of Health (R01 HL128349 and R01 HL151345). Dr. Matsuura is supported by the National Institute of Health (T32HL007843). Dr. Lefer was supported in part by the National Institutes of Health (1R01 HL146098, 1R56HL137711, 1R01 HL146514, and 1R01 HL151398). Drs. Sharp, Goodchild, and Lefer have a pending patent on the composition and methods for modeling HFpEF in Göttingen minipigs. All other authors

have reported that they have no relationships relevant to the contents of this paper to disclose.

ADDRESS FOR CORRESPONDENCE: Dr. David J. Lefer or Dr. Traci T. Goodchild, Cardiovascular Center of Excellence, Department of Pharmacology and Experimental Therapeutics, School of Medicine, Louisiana State University Health Science Center, 533 Bolivar Street, Suite 408, New Orleans, Louisiana 70112, USA. E-mail: dlefe1@lsuhsc.edu OR tgoodc@lsuhsc.edu.

PERSPECTIVES

COMPETENCY IN MEDICAL KNOWLEDGE: The increasing prevalence of HFpEF, coupled with a lack of effective therapies, represents a significant unmet need in cardiovascular medicine. The heterogeneity of the syndrome has created a challenging task to pinpoint the underlying mechanisms that drive human HFpEF. This is further exacerbated by a lack of preclinical models that effectively recapitulate the clinical scenario. To better understand the pathological drivers of HFpEF manifestation and progress, novel preclinical models must be developed.

TRANSLATIONAL OUTLOOK: The lack of good preclinical animal models that encompass the systemic, multiorgan dysfunction and comorbid-laden phenotype observed in patients has led to an inability to tease out mechanistic insights and test novel therapeutic strategies. Herein, we have developed a large animal model that integrates multiple comorbid determinants of HFpEF in a miniswine breed that exhibits sensitivity to obesity, metabolic syndrome, and vascular disease with overt clinical signs of heart failure. This model will allow for identification of key mechanisms and testing of novel therapeutic strategies, thereby permitting better clinical translation.

REFERENCES

1. Shah SJ, Borlaug BA, Kitzman DW, et al. Research priorities for heart failure with preserved ejection fraction. *Circulation* 2020;141:1001-26.
2. Zile MR, Gaasch WH, Carroll JD, et al. Heart failure with a normal ejection fraction: is measurement of diastolic function necessary to make the diagnosis of diastolic heart failure? *Circulation* 2001;104:779-82.
3. Shah SJ, Katz DH, Deo RC. Phenotypic spectrum of heart failure with preserved ejection fraction. *Heart Fail Clin* 2014;10:407-18.
4. Lourenço AP, Leite-Moreira AF, Balligand JL, et al. An integrative translational approach to study heart failure with preserved ejection fraction: a position paper from the Working Group on Myocardial Function of the European Society of Cardiology. *Eur J Heart Fail* 2018;20:216-27.
5. Pandey A, Vaduganathan M, Arora S, et al. Temporal trends in prevalence and prognostic implications of comorbidities among patients with acute decompensated heart failure: the ARIC Study Community Surveillance. *Circulation* 2020;142:230-43.
6. Hamdani N, Franssen C, Lourenço A, et al. Myocardial titin hypophosphorylation importantly contributes to heart failure with preserved ejection fraction in a rat metabolic risk model. *Circ Heart Fail* 2013;6:1239-49.
7. Schauer A, Draskowski R, Jannasch A, et al. ZSF1 rat as animal model for HFpEF: development of reduced diastolic function and skeletal muscle dysfunction. *ESC Heart Fail* 2020;7:2123-34.
8. He KL, Dickstein M, Sabbah HN, et al. Mechanisms of heart failure with well preserved ejection fraction in dogs following limited coronary microembolization. *Cardiovasc Res* 2004;64:72-83.
9. Lin J, Zhu X, Chade AR, et al. Monocyte chemoattractant proteins mediate myocardial microvascular dysfunction in swine renovascular hypertension. *Arterioscler Thromb Vasc Biol* 2009;29:1810-6.
10. Marshall KD, Muller BN, Krenz M, et al. Heart failure with preserved ejection fraction: chronic low-intensity interval exercise training preserves myocardial O₂ balance and diastolic function. *J Appl Physiol* 2013;114:131-47.
11. Ishikawa K, Aguero J, Oh JG, et al. Increased stiffness is the major early abnormality in a pig model of severe aortic stenosis and predisposes to

- congestive heart failure in the absence of systolic dysfunction. *J Am Heart Assoc* 2015;4:e001925.
12. Yarbrough WM, Mukherjee R, Stroud RE, et al. Progressive induction of left ventricular pressure overload in a large animal model elicits myocardial remodeling and a unique matrix signature. *J Thorac Cardiovasc Surg* 2012;143:215-23.
 13. Charles CJ, Lee P, Li RR, et al. A porcine model of heart failure with preserved ejection fraction: magnetic resonance imaging and metabolic energetics. *ESC Heart Fail* 2020;7:92-102.
 14. Gyöngyösi M, Pavo N, Lukovic D, et al. Porcine model of progressive cardiac hypertrophy and fibrosis with secondary postcapillary pulmonary hypertension. *J Transl Med* 2017;15:202.
 15. Kawase Y, Ly HQ, Prunier F, et al. Reversal of cardiac dysfunction after long-term expression of SERCA2a by gene transfer in a pre-clinical model of heart failure. *J Am Coll Cardiol* 2008;51:1112-9.
 16. Klein FJ, Bell S, Runte KE, et al. Heart rate-induced modifications of concentric left ventricular hypertrophy: exploration of a novel therapeutic concept. *Am J Physiol Heart Circ Physiol* 2016;311:H1031-9.
 17. Rienzo M, Bizé A, Pongas D, et al. Impaired left ventricular function in the presence of preserved ejection in chronic hypertensive conscious pigs. *Basic Res Cardiol* 2012;107:298.
 18. Weil BR, Techiryan G, Suzuki G, Konecny F, Canty JM. Adaptive reductions in left ventricular diastolic compliance protect the heart from stretch-induced stunning. *J Am Coll Cardiol Basic Trans Science* 2019;4:527-41.
 19. Zhang N, Feng B, Ma X, Sun K, Xu G, Zhou Y. Dapagliflozin improves left ventricular remodeling and aorta sympathetic tone in a pig model of heart failure with preserved ejection fraction. *Cardiovasc Diabetol* 2019;18:107.
 20. Schwarzl M, Hamdani N, Seiler S, et al. A porcine model of hypertensive cardiomyopathy: implications for heart failure with preserved ejection fraction. *Am J Physiol Heart Circ Physiol* 2015;309:H1407-18.
 21. Sorop O, Heinonen I, van Kranenburg M, et al. Multiple common comorbidities produce left ventricular diastolic dysfunction associated with coronary microvascular dysfunction, oxidative stress, and myocardial stiffening. *Cardiovasc Res* 2018;114:954-64.
 22. Borlaug BA, Carter RE, Melenovsky V, et al. Percutaneous pericardial resection: a novel potential treatment for heart failure with preserved ejection fraction. *Circ Heart Fail* 2017;10:e003612.
 23. van den Dorpel MMP, Heinonen I, Snelder SM, et al. Early detection of left ventricular diastolic dysfunction using conventional and speckle tracking echocardiography in a large animal model of metabolic dysfunction. *Int J Cardiovasc Imaging* 2018;34:743-9.
 24. Olver TD, Edwards JC, Jurrissen TJ, et al. Western diet-fed, aortic-banded Ossabaw swine: a preclinical model of cardio-metabolic heart failure. *J Am Coll Cardiol Basic Trans Science* 2019;4:404-21.
 25. von Scheidt M, Zhao Y, Kurt Z, et al. Applications and limitations of mouse models for understanding human atherosclerosis. *Cell Metab* 2017;25:248-61.
 26. Neeb ZP, Edwards JM, Alloosh M, Long X, Mokolke EA, Sturek M. Metabolic syndrome and coronary artery disease in Ossabaw compared with Yucatan swine. *Comp Med* 2010;60:300-15.
 27. Hand MS, Surwit RS, Rodin J, Van Order P, Feinglos MN. Failure of genetically selected miniature swine to model NIDDM. *Diabetes* 1987;36:284-7.
 28. Johansen T, Hansen HS, Richelsen B, Malmlof K. The obese Göttingen minipig as a model of the metabolic syndrome: dietary effects on obesity, insulin sensitivity, and growth hormone profile. *Comp Med* 2001;51:150-5.
 29. Ludvigsen TP, Kirk RK, Christoffersen BØ, et al. Göttingen minipig model of diet-induced atherosclerosis: influence of mild streptozotocin-induced diabetes on lesion severity and markers of inflammation evaluated in obese, obese and diabetic, and lean control animals. *J Transl Med* 2015;13:312.
 30. Renner S, Blutke A, Dobenecker B, et al. Metabolic syndrome and extensive adipose tissue inflammation in morbidly obese Göttingen minipigs. *Mol Metab* 2018;16:180-90.
 31. Segal JB, McNamara RL, Miller MR, et al. The evidence regarding the drugs used for ventricular rate control. *J Fam Pract* 2000;49:47-59.
 32. Sharp TE, Polhemus DJ, Li Z, et al. Renal denervation prevents heart failure progression via inhibition of the renin-angiotensin system. *J Am Coll Cardiol* 2018;72:2609-21.
 33. Douglas PS, Carabello BA, Lang RM, et al. 2019 ACC/AHA/ASE key data elements and definitions for transthoracic echocardiography: a report of the American College of Cardiology/American Heart Association Task Force on Clinical Data Standards (Writing Committee to Develop Cardiovascular Endpoints Data Standards) and the American Society of Echocardiography. *J Am Coll Cardiol* 2019;74:403-69.
 34. Sharp TE, Gong Z, Scarborough A, et al. Efficacy of a novel mitochondrial-derived peptide in a porcine model of myocardial ischemia/reperfusion injury. *J Am Coll Cardiol Basic Trans Science* 2020;5:699-714.
 35. Donnarumma E, Ali MJ, Rushing AM, et al. Zofenopril protects against myocardial ischemia-reperfusion injury by increasing nitric oxide and hydrogen sulfide bioavailability. *J Am Heart Assoc* 2016;5:e003531.
 36. Bradley JM, Islam KN, Polhemus DJ, et al. Sustained release nitrite therapy results in myocardial protection in a porcine model of metabolic syndrome with peripheral vascular disease. *Am J Physiol Heart Circ Physiol* 2015;309:H305-17.
 37. Böhm F, Pernow J. The importance of endothelin-1 for vascular dysfunction in cardiovascular disease. *Cardiovasc Res* 2007;76:8-18.
 38. Roh J, Houstis N, Rosenzweig A. Why don't we have proven treatments for HFpEF? *Circ Res* 2017;120:1243-5.
 39. Conceição G, Heinonen I, Lourenço AP, Duncker DJ, Falcão-Pires I. Animal models of heart failure with preserved ejection fraction. *Neth Heart J* 2016;24:275-86.
 40. Paulus WJ, Tschöpe C, Sanderson JE, et al. How to diagnose diastolic heart failure: a consensus statement on the diagnosis of heart failure with normal left ventricular ejection fraction by the Heart Failure and Echocardiography Associations of the European Society of Cardiology. *Eur Heart J* 2007;28:2539-50.
 41. Borlaug BA, Paulus WJ. Heart failure with preserved ejection fraction: pathophysiology, diagnosis, and treatment. *Eur Heart J* 2011;32:670-9.
 42. Pieske B, Tschöpe C, de Boer RA, et al. How to diagnose heart failure with preserved ejection fraction: the HFA-PEFF diagnostic algorithm: a consensus recommendation from the Heart Failure Association (HFA) of the European Society of Cardiology (ESC). *Eur J Heart Fail* 2020;22:391-412.
 43. Terris JM, Berecek KH, Cohen EL, Stanley JC, Whitehouse WM Jr., Bohr DF. Deoxycorticosterone hypertension in the pig. *Clin Sci Mol Med Suppl* 1976;3:303s-5s.
 44. Heinonen I, Sorop O, van Dalen BM, et al. Cellular, mitochondrial and molecular alterations associate with early left ventricular diastolic dysfunction in a porcine model of diabetic metabolic derangement. *Sci Rep* 2020;10:13173.
 45. Reddy YNV, Carter RE, Obokata M, Redfield MM, Borlaug BA. A simple, evidence-based approach to help guide diagnosis of heart failure with preserved ejection fraction. *Circulation* 2018;138:861-70.
 46. Ciccone CD, Zambraski EJ. Renal function in two-kidney deoxycorticosterone acetate-hypertensive Yucatan miniature swine. *Proc Soc Exp Biol Med* 1981;168:218-21.
 47. Zhang X, Lerman LO. Investigating the metabolic syndrome: contributions of swine models. *Toxicol Pathol* 2016;44:358-66.
 48. Valero-Muñoz M, Backman W, Sam F. Murine models of heart failure with preserved ejection fraction: a "fishing expedition". *J Am Coll Cardiol Basic Trans Science* 2017;2:770-89.
 49. Martin RJ, Gobble JL, Hartssock TH, Graves HB, Ziegler JH. Characterization of an obese syndrome in the pig. *Proc Soc Exp Biol Med* 1973;143:198-203.
-
- KEY WORDS** animal models of human disease, obesity, metabolic syndrome, hypertension, heart failure with preserved ejection fraction